Chemically Resolved Photovoltage Measurements in CdSe Nanoparticle Films†

Hagai Cohen,*,‡ Shaibal K. Sarkar,§ and Gary Hodes§

Department of Chemical Research Support, and Department of Materials and Interfaces, The Weizmann Institute of Science, Rehovot 76100, Israel

Received: July 29, 2006; In Final Form: September 21, 2006

Light-induced chemically resolved electrical measurements (CREM) under controlled electrical conditions are used to study photovoltaic effects at selected regions in nanocrystalline CdSe-based films. The method, based on X-ray photoelectron spectroscopy (XPS), possesses unique capabilities for exploring charge trapping and charge transport mechanisms, combining spectrally filtered input signals with photocurrent detection and with a powerful, site-selective, photovoltage probe.

Introduction

X-ray photoelectron spectroscopy (XPS) has become a widely used tool in materials research, due to its high surface specificity and sensitivity to the chemical state of individual elements. Upon irradiation with a monochromatic X-ray beam, photoelectrons are emitted from the sample, and their kinetic energy (E_k) can be used to deduce the electron binding energy (BE). The kinetic energy of the photoelectrons is also influenced by electrostatic effects, such as charging of the sample surface.[1−6] To prevent this most often undesirable effect (although useful structural information has been successfully extracted from differential charging effects[7−11]), low energy electrons are usually applied to the surface from an electron flood gun (eFG), to compensate this extra positive charge. Besides electron beam neutralization, visible light illumination[12] has also been used for the suppression of charging in poorly conducting systems.

Several attempts to derive electrical information from these effects have been reported as well,[7,13−22] including light-induced photoemission spectroscopy (LIPES) demonstrating photoconductivity and band bending changes in semiconductors.[16−18] Recently, incorporating sample current detection, an approach to chemically resolved electrical measurements (CREM) has been proposed,[19] providing unique capabilities, for example, the elimination of contact difficulties in DC measurements, performance of $I-V$ curves at selected subsurface regions, and work-function derivation.[20,21]

In this paper, we describe a comprehensive methodology for chemically resolved photovoltaic (CRPV) measurements, combining: (1) detection of surface electrical potential variations; (2) sample current measurements (from sample to earth) with only one (back) electrical contact needed; (3) electrical input signals applied via three independent external sources (the power of the X-ray source itself, application of an external electrical field by a nearby grid, and an electron flood gun (eFG) as an external source of current); and (4) optical excitation. The experiments shown below are aimed at a general assessment of the method's potential and capabilities, presenting photovoltaic effects in thin overlayers of CdSe nanoparticles. In a recent publication,[23] we have described unusual photoactivity of such layers deposited on silicon wafers. Real-time internal field switching via illumination intensity and/or application of external electrical fields has been demonstrated. Here, we build on this earlier work, presenting new experimental data and methodological improvements. A top retarding grid and two separated light sources are used to achieve fine control of the external electrical signal and charge generation. With the resulting improvement in CRPV sensitivity, we demonstrate differentiation of charge trapping from transport mechanisms in porous, nanocrystalline semiconducting films.

Experimental Section

Sample Preparation. Si substrates (single crystal ⟨100⟩, arsenic doped n-type), either highly doped (resistivity in the range 0.001−0.005 Ω cm) or medium doped (ca. 1 order of magnitude higher resistivity), were etched by immersion in 50% v/v 40% HF (i.e., in 20% aqueous solution of HF) for 3 min and then rinsed well with water. CdSe deposition was carried out by chemical bath deposition following the procedures described elsewhere.[23] The solutions were composed of $CdSO_4$, the K salt of nitrilotriacetic acid (as complexant for Cd), and Na_2SeSO_3. Deposition was carried out at 10 °C in the dark giving a crystal size of ca. 4 nm.

Depending on preparation details, the Cd:Se stoichiometry was >1, reflecting a $Cd(OH)_2$-rich layer at the substrate[23] and possibly also some loss of SeO_2 (from oxidized surface CdSe) in the vacuum of the XPS spectrometer.[24] Residual carbon and oxygen were always seen. Sample stability under the beam was investigated for time periods up to 12 h irradiation, in several cases exhibiting significant changes in the photoresponse. The data presented below correspond to relatively short exposures, where such changes were small.

The Cu-doped CdSe was deposited in the same way but adding CuCl to the deposition solution with a $[Cu^{2+}]$:$[Cd^{2+}]$ ratio of 0.01 (i.e., nominal doping concentration of 1%). The actual concentration in the sample (measured by XPS) was 1.8%. Detailed characterization of this system has suggested Cu enrichment at the surface of the CdSe nanoparticles,[25] where the chemical state of the Cu is Cu^{1+}, probably Cu_2Se: $Cu(2p_{3/2})$ binding energy of 931.9 eV and Auger (LMM) kinetic energy of 917.6 eV, see also literature data for Cu_2Se.[27]

XPS/CREM Characterization. Measurements were performed on a slightly modified Kratos AXIS-HS setup, using a

† Part of the special issue "Arthur J. Nozik Festschrift".

* Corresponding author. E-mail: hagai.cohen@weizmann.ac.il.
‡ Department of Chemical Research Support.
§ Department of Materials and Interfaces.

10.1021/jp0648590 CCC: $33.50
Published on Web 11/15/2006

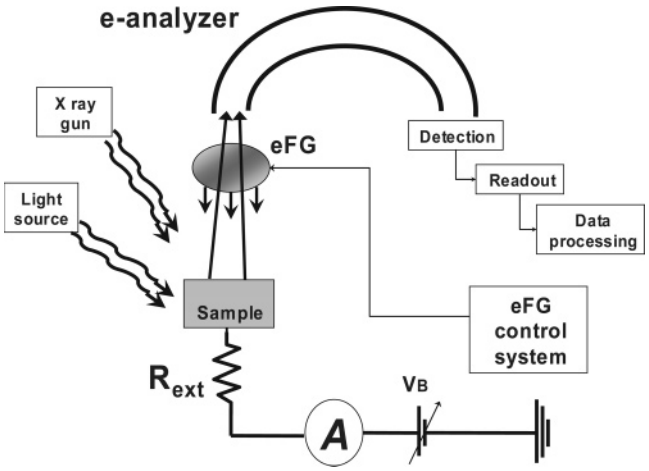

Figure 1. The experimental setup: A schematic illustration of the X-ray photoelectron spectrometer, equipped with a source for light illumination and a picoammeter (A) for the detection of sample current. The electron flood gun (eFG) includes, in addition to its electron emitting filament, a grid which can effectively vary the X-ray-induced outgoing current of secondary electrons.

monochromatic Al(K_α) source at 75 W. The electrical input was supplied with an electron flood gun (eFG) controlled via two negative bias voltages, V_F and V_G, and via filament current, I_F, the latter varied between 1.55 and 2.0 A. The eFG bias voltages ranged from 0 to 4.6 V. Two light sources were used: a HeNe laser ($\lambda = 632.8$ nm; intensity at the sample equivalent to a current of ca. 13 mA cm^{-2} measured by a Si photodiode) and a halogen lamp (ca. 0.8 mA cm^{-2} by the Si photodiode). Various filters were added to the halogen source, mainly low-pass and neutral density filters. XPS line shifts were determined via numerical shifts of the data,[10,19] a procedure based on the correlation of many data points, therefore capable of improved resolution, down to ca. 10 meV, and in certain cases even better. The current through the sample was detected with a Keithley 487 pico-ammeter connected between the back contact of the sample and earth. A schematic description of the experimental setup is given in Figure 1.

Surface Photovoltage (SPV) Measurements. SPV measurements were made using a commercially available Kelvin probe (Besocke, Delta-Phi) with a sensitivity of ~1 mV and a vibrating gold reference. The sample was illuminated via a 600 W Xe lamp passing through a 0.5 m grating monochromator (Jobin-Yvon 270M).

It should be noted that all SPV measurements were carried out in ambient atmosphere, while the XPS ones were made in an ultrahigh vacuum.

Results and Discussion

In the following, we define a flow of electrons from the surface to the back contact as a negative current. Also, we adopt a potential definition, which retains the sign of energy levels: that is, positive potentials (higher energy levels) for negative charging. Denoting "p-like" ("n-like") behavior means that the CdSe layer (which is actually intrinsic) exhibits a photocurrent/photovoltage of the same sign as would a p-type (n-type) semiconductor: positive photovoltage values for p-type semiconductors (negative values for n-type samples). Note that because the substrate is grounded, "n-type" response appears as a downward shift of the surface levels and not an upward shift of the substrate Fermi level, as would normally occur in a photovoltaic cell.

Figure 2a describes a crude spectral analysis where both the photovoltage and the photocurrent of a ~10 nm thick CdSe film on degenerate n-Si are measured, using low-pass cutoff filters at the exit of the halogen lamp. With a suitable setup, this could be done much more accurately using a monochromator. However, the essential features of this measurement can be seen: an increasing photoresponse magnitude (ΔV and ΔI) with increasing photon energy (decreasing wavelength), up to the CdSe band gap (ca. 570 nm in this sample), and decreasing photoresponse at shorter wavelengths (above the band gap).

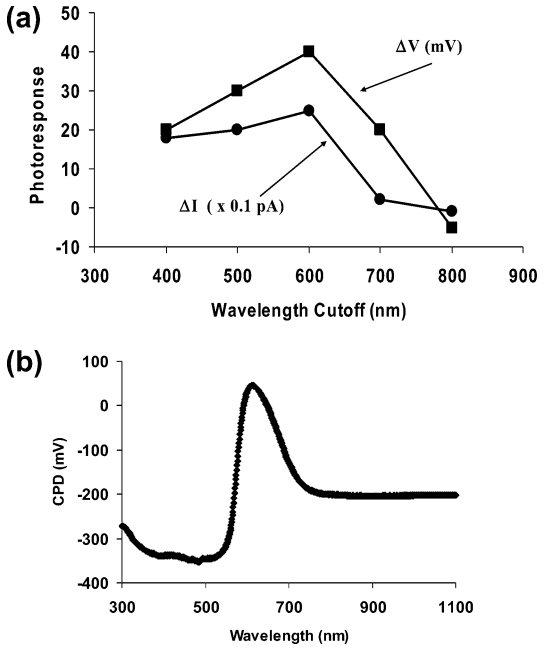

Figure 2. Wavelength dependence of the photoresponse: (a) CREM-derived photocurrent and photovoltage, using low pass filters at the exit of the halogen lamp; (b) Kelvin probe detection of the contact potential difference using monochromated light source. Samples are 10−15 nm thick. Note that the "p-type" response starts far below the energy gap of the nanoparticles (absorption edge at ~570 nm) and that n-type contributions "switch on" at ~620 nm, just below the energy gap of the nanoparticles.

Figure 2b shows an independent Kelvin probe surface photovoltage (SPV) measurement. The contact potential difference (CPD) variation upon illumination is measured here as a function of monochromatic light wavelength. The spectrum in Figure 2b essentially corresponds to the derivative of the low-pass filtering used in Figure 2a, as indeed obtained experimentally. One can further verify that this behavior does not originate in substrate photoresponse. As demonstrated in Figure 3, the conductive substrate in these samples (the Si, Figure 3b) retains a practically fixed potential under light illumination (white light in this specific case), while the Cd line (Figure 3a) exhibits a measurable (and reversible, not shown) shift, which reflects the change in surface potential.

A clear "p-type" response, beginning at ca. 780 nm, is manifested in the low-energy region of Figure 2a and b, far below the energy gap of the CdSe particles, whereas a second mechanism switches on around 620 nm, introducing an increasing "n-type" tendency. The Kelvin probe data, Figure 2b, are fully consistent with the XPS-based results, obviously with improved spectral quality enabled by the monochromatic input signal. The photocurrent in Figure 2a follows, as expected, the direction of the photovoltage: accumulation (depletion) of negative surface charge is naturally accompanied by positive (negative) photocurrent, i.e. an increase (decrease) in the current of holes toward ground.

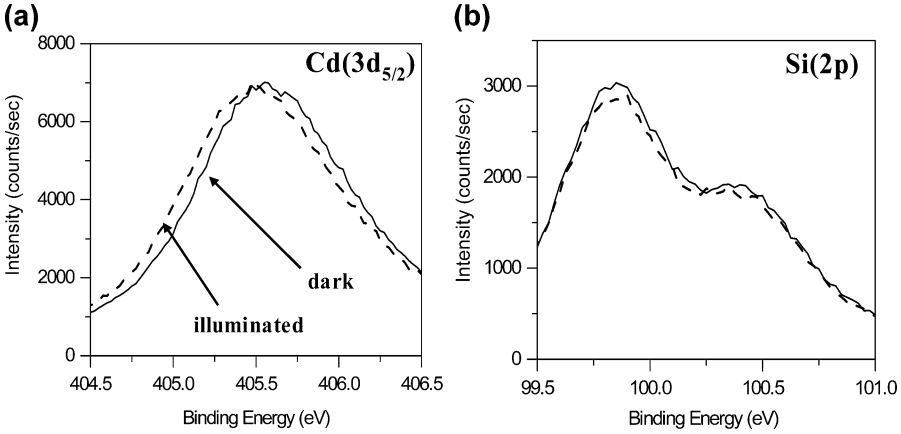

Figure 3. Demonstration of light-induced XPS shifts: (a) the overlayer Cd($3d_{5/2}$) line; (b) the substrate Si(2p) line. The Cd shift (under halogen light) is "p-type", i.e. a shift to higher kinetic energy (lower binding energy). The Si line does not shift, verifying that this highly conducting substrate retains a fixed potential at the interface.

TABLE 1: XPS-Based Photovoltage Measurements Studied with Two Light Sources: a Red HeNe Laser and a White Halogen Light, Recorded from a ~10 nm Thick CdSe Overlayer on a Medium-Doped, n-Si Wafer[a]

	HeNe	halogen	HeNe+halogen	halogen net
Cd	−100	−60	−85	+15
Si	−170	−50	−130	+40
Cd-net	+70	−10	+45	−25

[a] All photovoltage numbers are given in mV. The halogen net column presents the response to halogen illumination when the HeNe laser is already switched on. Note that the top surface potential floats on that of the grounded substrate, the latter directly probed via the Si($2p_{3/2}$) line, which can, therefore, be used to extract the actual photovoltage across the overlayer (Cd-net). Note also that the substrate response to halogen, typically of negative values (as expected for n-type semiconductors), becomes positive when the HeNe laser is already switched on.

We interpret the results as an onset of electron trapping at deep states of the film, ~780 nm, and a switchover to dominant (shallow) hole trapping at ~620 nm, just below the CdSe energy gap. This is in line both with earlier SPV studies of nanocrystalline semiconductor films[26] and with our previous study of this system[23] (even though the rich details resolved in Figure 2 were not observable in Figure 6 of ref 23, where thicker layers were examined). Two types of traps, spatially separated, were suggested in ref 23 to coexist in the system and, hence, to provide real-time shaping capabilities of its internal electrical field. The proposed model structure included a low density of deep electron traps and a large number of shallow hole traps. As a result of the competing trapping mechanisms, the spectral response of these CdSe nanocrystalline layers can vary considerably depending on externally controllable factors.[23] It can be either "p-" or "n-type" and can switch from one to the other via electrical input signals and/or variations in light intensity. The present photovoltage (and photocurrent) measurements in Figure 2 provide direct support for our previous hypothesis.

Further insight on the mechanisms involved in the photocharge excitation may be gained by resolving photovoltaic effects at different spatial locations, a unique capability of CREM, best examined in samples consisting of two photoactive regions. A relatively thin layer (ca. 10 nm average thickness) on nondegenerate n-Si is studied, while two light sources are applied.[28] Table 1 presents the photovoltages under different illumination conditions (HeNe laser, halogen lamp, and both sources together).

Looking first at the Si signal, negative photovoltage is obtained under red light (see Table 1), typical of band bending (BB) flattening in n-type semiconductors. Under white light the substrate photovoltage is also negative, although of smaller magnitude. However, when (the same) white light source is added to the HeNe illumination, the silicon line undergoes an opposite (positive) shift (from −170 to −130 mV). The resulting change in substrate potential, given by the last column in Table 1 (halogen net), $\Delta\phi = +40$ mV, opposes the BB flattening in this n-type silicon.

Normally, one does not expect high added sensitivity (at most, a small negative shift) of the substrate to the halogen illumination in this two-beam experiment. This is because of the logarithmic dependence of photovoltage on light intensity. The above unusual result can, however, originate in light absorption at the neighboring CdSe overlayer: Electron−hole excitation at the CdSe is switched on at the short wavelength regime of the halogen light, supplying electrons to refill the Si/CdSe interface traps and, hence, suppressing the BB flattening.

The Cd data complement this explanation. Recalling that the overlayer potential floats on that of the substrate, the Cd-net line in Table 1 provides the actual potentials developed across the overlayer itself. Under red light, the Cd-net photovoltage (last row in Table 1) is positive, indicating that either subband gap response takes place in the CdSe particles or, alternatively, that electrons are injected from the substrate to the overlayer. Both mechanisms would lead to a similar "p-type" response, in full agreement with our data in Figure 2. In contrast, and again in agreement with Figure 2, upon short wavelength illumination (see last column in Table 1), when e−h excitation is switched on at the nanoparticles, the net overlayer photovoltage becomes negative (−25 mV), characteristic of "n-type". The general aspect to be stressed here is that mutual influence of two photoactive domains, the substrate and the overlayer, has been resolved in this two-beam experiment: electron injection from the CdSe to the interface taking place at short wavelengths, and injection from the substrate to the overlayer at long wavelengths.

The above experiment demonstrates, as already mentioned, an important capability of the CREM approach: performing the SPV analysis on different spectral lines and consequently resolving photovoltage values at specific locations, usually (yet not limited to) locations of well-defined chemical identity. Thus, the chemical probe can be exploited as well to gain insight on the role of dopants within or on photoactive matrixes. An example is shown in Table 2, where a 1.8% Cu-doped CdSe overlayer on n-Si substrate is exposed to halogen light. Positive photovoltage values are observed in this system too, associated

TABLE 2: Photovoltage (in mV) Observed under Halogen Light Illumination for 1.8% Cu-Doped CdSe Nanoparticles[a]

Cd	Se	O	C	Cu
20	20	10	25	100

[a] All values are positive, corresponding to a "p-type" behavior (dominant e-trapping). Note the significantly high value obtained at the Cu doping sites.

with accumulation of surface negative charge (electron trapping). Interestingly, the shift of the Cu line is much greater than the Cd and Se shifts, providing a direct indication for enhanced light-induced electron trapping at the Cu sites.

We next examine the photoresponse as a function of external electrical signals. In general, the interpretation of these measurements is not trivial. We therefore start here with a relatively simple situation, where the eFG is not in use. The CREM analysis necessarily involves finite dark currents due to the x-irradiation, here referred to as the positive charging regime (electrons are ejected to the vacuum). Under eFG-off conditions, when this current of X-ray ejected electrons cannot be neglected, it can be finely controlled by (1) varying the power of the X-ray gun (emission current 1−5 mA) and (2) by applying negative bias (0−30 V) to the eFG grid (the eFG filament still switched off) and, hence, repelling back a controllable portion of the outgoing secondary electrons.[29]

Under light illumination, a positively charged surface is subjected to at least two mechanisms: (1) photoconductivity, that is, the improvement in hole transport to ground, and (2) trapping of photoexcited charges. Can one differentiate the ohmic from the capacitive mechanism? Generally speaking, charge-trapping dynamics would intermix those classical limits. However, in the following experiment (Figure 4a,b), by correlating photocurrent (ΔI) and photovoltage (ΔV), we obtain well-separated regimes. Data points with practically no photocurrent are associated mainly with space charge evolution (electron trapping), while the others involve ohmic photoconductivity as well. Three data sets are presented in Figure 4a, exhibiting a simple relation between ΔI and I, while the grid and x-emission parameters are varied: (1) ◆ symbols represent photoresponse data under a low x-source emission current of 1 mA and grid voltages (V_G) varied between −30 V (the lowest current data point) and 0 V (highest current); (2) ■ symbols again represent V_G variations, but at 2 mA emission of the x-gun; and (3) △ present three data points with the x-emission varied from 3 to 5 mA (the high current points) under $V_G = 0$, plus a single test point (▲) recorded at 5 mA and $V_G = -30$ V.

To a first-order approximation, all data points in Figure 4a fall on a common linear curve, a behavior typical to photoconductivity: the light signal is identical for all data points, and, hence, the induced change in resistance, ΔR, would roughly retain a constant ratio $\Delta I/I$. It is noted, however, that under low dark current conditions, the slope of the curve is not retained, suggesting that additional mechanisms should be considered here.

Complementary information is provided by Figure 4b, where even under highly suppressed currents (and photocurrents), significant photovoltage values are detected (transient currents will not be seen in these steady-state measurements). All data points in Figure 4b were measured simultaneously with those of Figure 4a. Hence, the experiment suggests that, in addition to photoconductivity, charge trapping is important here, becoming the dominant process at the low current regime in Figure 4b. Recalling that these slow measurements correspond to the steady-state limit, we consider a simplified classical description

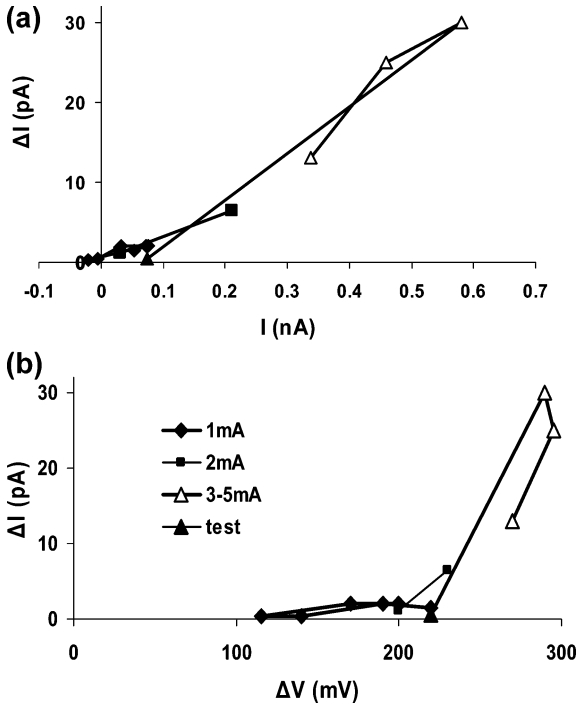

Figure 4. The photoresponse under controlled positive charging conditions, measured for halogen light illumination: (a) photocurrent versus dark current; (b) photocurrent versus photovoltage. Two parameters dictate the electrical conditions: the X-ray flux (via emission current, I_X); and a grid situated above the sample, its negative bias (V_G: 0−30 V) acting to repel the X-ray ejected low-energy photoelectrons, thus controlling the integral dark current and the positive charging magnitude. ◆ symbols are measured for variable V_G at $I_X = 1$ mA; ■ symbols represent varied V_G at $I_X = 2$ mA; varying I_X between 3 and 5 mA is given by the triangles, with the △ for $V_G = 0$ V and the ▲ as a test measured at 5 mA and −30 V. Note the clear differentiation of photoconductivity from the effect of charge trapping, the former characterized by correlated $\Delta I - \Delta V$, while the latter appears with minimal current variations.

of the system, with independent ohmic (V_R) and capacitive (V_C) potentials:

$$V = V_R + V_C = I \cdot R + \frac{Q}{C} \tag{1}$$

where Q is the accumulated surface charge and C is the layer capacitance. The variation of the ohmic term under light signal becomes:

$$\Delta V_R = \Delta I \cdot R + I \cdot \Delta R \tag{2}$$

which yields:

$$\frac{\Delta V_R}{V_R} = \frac{\Delta R}{R} + \frac{\Delta I}{I} \tag{3}$$

$\Delta I/I$ as derived from Figure 4a (the high current regime) is about 0.06; $\Delta V_R/V_R$ is similarly found (not shown) to be ∼0.4; and R is roughly 0.66 GΩ. Thus, a CREM estimated value, $\Delta R \approx 0.23$ GΩ, is obtained for the specific white light illumination used in this experiment.

The capacitive term, ΔV_C , is mainly related to the space charge accumulation, ΔQ (provided that the capacitance does not vary). Based on our previous work,[23] as well as on the data in Figure 2 and Table 1, two trapping mechanisms should be considered for the space charge accumulation: electron capture in traps located at the overlayer/substrate interface, and hole

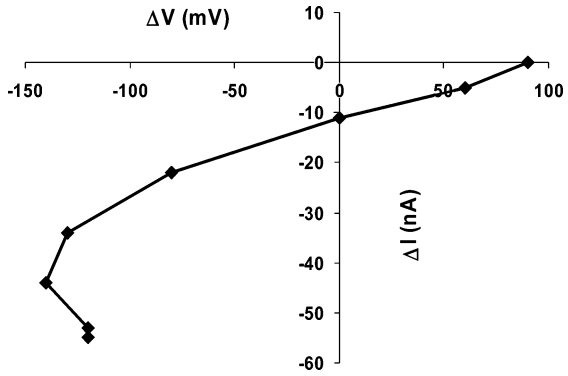

Figure 5. Photoresponse variations under controlled negative charging conditions: photocurrent versus photovoltage characteristics measured under halogen illumination and electrical input signals varied via the eFG voltages: $V_G = 1.5V_F$, where V_F is a floating potential set at the eFG filament. Note how the photovoltage, which is positive ("p-type" behavior) under low eFG conditions, gradually switches to a negative ("n-type") behavior. The dark current at the crossover is −11.6 nA.

trapping within the CdSe layer. Under dark positive charging conditions, only hole traps can be populated, their filling believed to roughly follow the magnitude of the dark current. Therefore, when the (initial) dark current is strongly suppressed (low x-emission, high V_G in Figure 4), "p-type" contributions to the photoresponse necessarily arise from the filling of electron traps (at the interface). This mechanism yields here $\Delta V_C \approx 120$ mV (see Figure 4b) and, accordingly, a practically zero (steady-state) photocurrent. For a finite positive dark current, when hole traps are initially populated, a second mechanism emerges: photoexcited electrons annihilate the trapped holes (on a short time scale) and hence add to the "p-type" photovoltage another ~100 mV, as can be judged from the intermediate region in Figure 4b. In this case, the (steady-state) photocurrent is not zero, but still small. Finally, as already explained above, at even higher dark currents, photoconductivity becomes a third important mechanism.

It is stressed that charge trapping and photoconductivity act here in the same direction, contributing positive ΔV and positive ΔI values (due to electron trapping and/or improved removal of holes). The clear differentiation of these mechanisms, seen in Figure 4, is not an easy task for standard electrical means. In principle, it could be done by high frequency measurements, but this would require modeling of the system, with the danger of misinterpretation. The advantage of the CREM probe arises from the fact that it can directly measure potentials actually developing at the surface, in contrast to an externally applied value associated with the electrode (contact) and not necessarily the sample itself. More specifically, Figure 4 provides strong support for the significant role of electron trapping in this system, an assumption made in our previous study.[23] This follows from the capacitive behavior in Figure 4b, that is, change in potential with practically no change in (steady-state) current (see the 1 mA emission current plot, and the extrapolation of the other two plots to $\Delta I = 0$, where ΔV retains a fairly large value).

The study under controlled electrical loads can now be extended by activating the electron flood gun (eFG). Figure 5 presents the photocurrent versus photovoltage of a "p-type" CdSe/Si system (similar to the one studied in Figure 4) under increasing eFG flux (low eFG flux on the right side, and high flux on the left). Significant variations in ΔV are observed, where, strikingly, ΔV even changes its sign at a certain point, switching from "p-like" to "n-like" behavior. This effect has been previously observed in plots of photovoltage versus sample current (rather than photocurrent shown here) and in complementary Kelvin probe measurements (Figures 8 and 3, respectively, in ref 23). At elevated eFG flux, a maximum is observed in the photovoltage, a feature explained by the interaction of eFG electrons with holes trapped in the CdSe layer. This latter point, associated with the physics of ballistic electron interactions, will be dealt in a future publication.[29] Probing specific charge trapping mechanisms via application of both eFG and optical signals is likely to be of particular help in future studies of charge dynamics.

While we have implied certain similarities between these CREM and conventional photoelectrical measurements, it is important to stress (in some cases repeat) the differences. These are listed below.

(1) The sample is tied to ground. Changes in surface potential, for example, due to changes in band bending, would be seen in an energy diagram as a change in band edge at the semiconductor surface and not by a change in Fermi level at the electrical contact.

(2) There is no direct electrical contact to the sample surface. In this respect, this is closer to an open circuit system. The X-ray-induced (dark) current (a photocurrent by itself, which should not be confused with the light-induced photocurrent) can be assumed here to have no (or negligible) sensitivity to the optical signals. The light-generated charges are thus removed at one side only of the "device" (the substrate contact).

(3) Electrons injected from the flood gun are not injected at the Fermi level, as is the case for conventional electron injection through a contact, but at a higher energy (the vacuum level or higher). The energy of the electrons above the vacuum level can be controlled. Photoelectrons as well, repelled by a negative grid, are re-injected at the vacuum level or above.

Conclusions

Chemically resolved photovoltaic measurements have been shown to provide unique capabilities as a probe of semiconductor structures. Using nanocrystalline samples with two or more spatially separated domains, we have demonstrated a few of the wide range of measurements possible with this technique. The photoresponse could be selectively probed at different regions and different chemical sites of the system. Applying a double beam optical source, or spectral filtering of the input light signals, under controlled electrical constraints as an additional input signal, detailed accessibility to charge transport and charge trapping mechanisms in porous, nanocrystalline, semiconducting films has been demonstrated.

Acknowledgment. We thank Leeor Kronik for fruitful discussions. The work was supported by the Israel Science Foundation and the G. M. J. Schmidt Minerva Center for Supramolecular Architectures.

References and Notes

(1) *Practical Surface Analysis*, 2nd ed.; Briggs, D., Seah, M. P., Eds.; Wiley: New York, 1990; Vol. 1.
(2) Barr, T. L. *J. Vac. Sci. Technol., A* **1989**, *7*, 1677.
(3) Lewis, R. T.; Kelley, M. A. *J. Electron Spectrosc. Relat. Phenom.* **1980**, *20*, 105.
(4) Wagner, C. D. *J. Electron Spectrosc. Relat. Phenom.* **1980**, *20*, 105.
(5) Windawi, H.; Wagner, C. D. In *Applied Electron Spectroscopy for Chemical Analysis*; Windawi, H., Ho, F. F. L., Eds.; John Wiley and Sons: New York, 1982; p 191.
(6) Cazaux, J. *J. Electron Spectrosc. Relat. Phenom.* **1999**, *105*, 155.
(7) Lau, W. M. *Appl. Phys. Lett.* **1989**, *54*, 338.
(8) Miller, J. D.; Harris, W. C.; Zajac, G. W. *Surf. Interface Anal.* **1993**, *20*, 977.

(9) Shabtai, K.; Rubinstein, I.; Cohen, S. R.; Cohen, H. *J. Am. Chem. Soc.* **2000**, *122*, 4959.
(10) Doron-Mor, I.; Hatzor, A.; Vaskevich, A.; van der Boom-Moav, T.; Shanzer, A.; Rubinstein, I.; Cohen, H. *Nature (London)* **2000**, *406*, 382.
(11) Feldman, Y.; Zak, A.; Tenne, R.; Cohen, H. *J. Vac. Sci. Technol., A* **2003**, *21*, 1752.
(12) Buller, R.; Cohen, H.; Minkin, E.; Popovitz-Biro, R.; Lifshitz, E.; Lahav, M. *Adv. Funct. Mater.* **2002**, *12*, 713.
(13) Lau, W. M. *J. Appl. Phys.* **1989**, *65*, 2047.
(14) Lau, W. M. *J. Appl. Phys.* **1990**, *67*, 1504.
(15) Lau, W. M.; Wu, X. W. *Surf. Sci.* **1991**, *245*, 345.
(16) Hecht, M. H. *Phys. Rev. B* **1990**, *41*, 7918.
(17) Long, J. P.; Bermudez, V. M. *Phys. Rev. B* **2002**, *66*, 121308/1.
(18) Bandis, C.; Pate, B. B. *Surf. Sci.* **1996**, *345*, L23.
(19) Cohen, H. *Appl. Phys. Lett.* **2004**, *85*, 1271.
(20) Ray, S. G.; Cohen, H.; Naaman, R.; Liu, H. Y.; Waldeck, D. H. *J. Phys. Chem. B* **2005**, *109*, 14064.
(21) Cohen, H.; Nogues, C.; Zon, I.; Lubomirsky, I. *J. Appl. Phys.* **2005**, *97*, 113701/1.
(22) Cohen, H.; Zenkina, O. V.; Shukla, A. D.; van der Boom, M. E. *J. Phys. Chem. B* **2006**, *110*, 1506.
(23) Sarkar, S. K.; Cohen, H.; Hodes, G. *J. Phys. Chem. B* **2005**, *109*, 182.
(24) Katari, J. E. B.; Colvin, V. L.; Alivisatos, A. P. *J. Phys. Chem.* **1994**, *98*, 4109.
(25) Gorer, S.; Chandrasekharan, N.; Hodes, G., unpublished results.
(26) Kronik, L.; Ashkenasy, N.; Leibovitch, M.; Fefer, E.; Shapira, Y.; Gorer, S.; Hodes, G. *J. Electrochem. Soc.* **1998**, *145*, 1748.
(27) *Handbook of X-ray Photoelectron Spectroscopy*; Jill, C., Ed.; Perkin-Elmer Corp.: Minnesota, 1992.
(28) At such thickness, the granular structure of the film may result in regions of uncoated Si.
(29) Cohen, H., in preparation.